A Family of Frontal Cyclones over the Western Atlantic Ocean. Part II: Parameter Studies

DA-LIN ZHANG

Department of Meteorology, University of Maryland, College Park, Maryland

EKATERINA RADEVA AND JOHN GYAKUM

Department of Atmospheric and Oceanic Sciences, McGill University, Montreal, Quebec, Canada

(Manuscript received 20 April 1998, in final form 14 August 1998)

ABSTRACT

In this study, a series of sensitivity experiments is performed to study the relative influence of latent heating, surface friction, and surface heat fluxes on the development of a family of frontal cyclones that occurred over the western Atlantic Ocean, using the simulation presented in Part I as a control run. It is shown that dry dynamics determines the initiation and track of all the frontal cyclones, and it accounts for about 59% of the deepening of a major frontal cyclone. Vorticity budget calculations reveal that in the absence of latent heating, preexisting upper-level cyclonic vorticity associated with a ring of potential vorticity provides the necessary forcing for the initiation and movement of the frontal cyclones, whereas the low-level thermal advection is responsible for a large portion of their amplifications as well as for their shallow circulations.

The impact of surface sensible and latent heat fluxes on the frontal cyclogenesis depends on the cyclones' location with respect to the warm water surface. In the absence of latent heating, the surface fluxes have very weak impact, through modifying the low-level baroclinicity, on the evolution and final intensity of the frontal cyclones. When latent heating is allowed, however, the surface fluxes could result in more rapid cyclogenesis as a result of reduced static stability and increased moisture content in the maritime boundary layer; the impact is as pronounced as the latent heating. It is found that (dry) frontal cyclogenesis could still occur over a vast continental surface, although it is the slowest moving and deepening system among all the sensitivity tests being conducted.

The results reveal that (i) the frontal cyclones in the present case are baroclinically driven in nature, although they are markedly modulated by diabatic heating and surface fluxes; and (ii) the rapid frontal cyclogenesis phenomena tend to occur more frequently over a warm ocean surface due to its associated weak surface friction and its generated weak static stability in the maritime boundary layer.

1. Introduction

There has been considerable progress in the past decades on the understanding and numerical prediction of extratropical cyclogenesis, especially those rapidly deepening oceanic storms that occurred at a scale of greater than the Rossby radius of deformation or 3000 km (the so-called large-scale cyclogenesis). A comprehensive review of the advances in knowledge by theoretical, observational, and modeling approaches was published following the Palmén Memorial Symposium (Newton and Holopainen 1990). Previous studies have clearly shown the importance of diabatic heating (stratiform and convective), surface characteristics, the air–sea interaction, and other physical processes in determining the final intensity of oceanic cyclones, although their relative significance varies from case to case (Kuo and Low-Nam 1990). In particular, numerical sensitivity studies have led to the recognition that individual physical and dynamical processes are not sufficient, when acting in isolation, to produce rapid cyclogenesis despite the presence of extremely intense baroclinicity.

In contrast, little work has been done to gain insight into the relative importance of various physical processes in frontal cyclogenesis that often begins as a mesoscale vortex (i.e., with a diameter of a few hundreds kilometers) embedded in a large-scale (parent) cyclone. This is primarily due to the fact that this type of cyclogenesis occurs at relatively too small scales and often over data-void oceans. Because of the limited knowledge on frontal cyclones, the Fronts and Atlantic Storm Track Experiment (FASTEX; Snyder 1996; Joly et al. 1997) was recently conducted in hope of providing necessary high-resolution data to attack the frontal cyclo-

Corresponding author address: Dr. Da-Lin Zhang, Department of Meteorology, University of Maryland, Room 2213, Space Science Building, College Park, MD 20742-2425.
E-mail: dalin@atmos.umd.edu

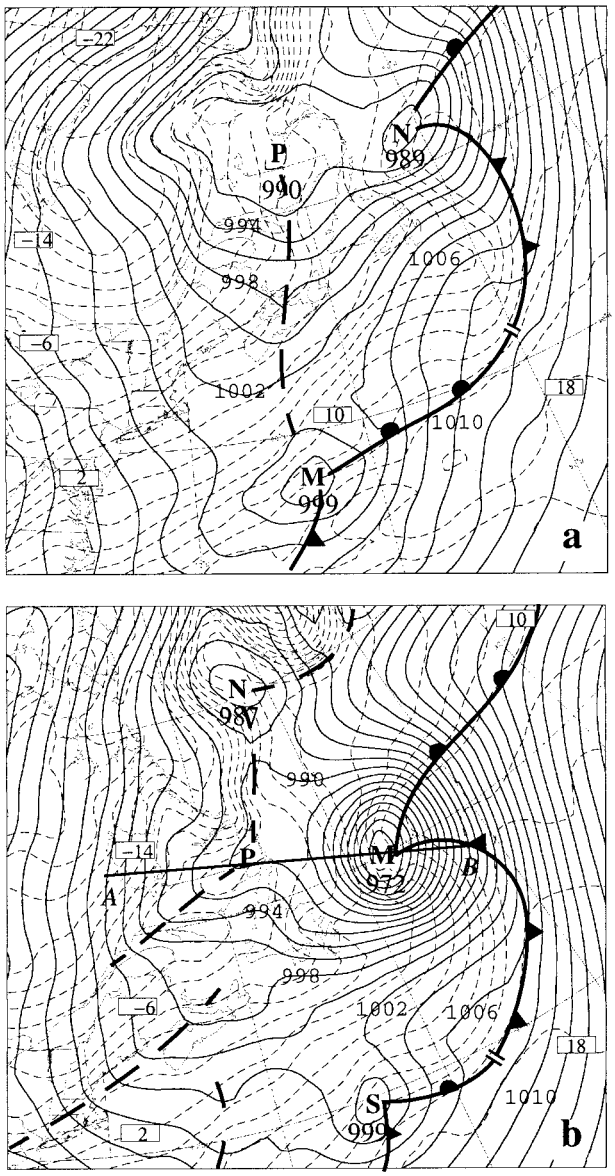

FIG. 1. Sea level pressure (solid, every 2 hPa) and surface temperature (dashed, every 2°C) from (a) 24- and (b) 48-h control simulations (expt CTL). P, M, N, and S denote the center of the parent, major, northern, and southern frontal cyclones, respectively.

genesis problem. One of the objectives of FASTEX was to clarify the relative importance of some dynamical processes and latent heat release in frontal cyclogenesis (Snyder 1996).

In Part I of this series of papers (Zhang et al. 1999), we have presented a 60-h simulation and analysis of a family of six such systems that formed over the western Atlantic Ocean during 13–15 March 1992 using the Pennsylvania State University–National Center for Atmospheric Research mesoscale model with a fine-mesh grid size of 30 km. For the convenience of later discussions, Fig. 1 shows two surface maps of the frontal cyclone family that are taken from 24- and 48-h simulations, valid at 0000 UTC 14 March and 0000 UTC 15 March 1992 (henceforth 14/00–24, 15/00–48), respectively. The two periods are chosen because they represent the incipient and mature stages of the oceanic storm. It is apparent from Fig. 1 that the model produces three frontal cyclones at 15/00–48: the northern (NFC), major (MFC), and southern (SFC) ones, as marked by N, M, and S, respectively. Of importance is that the MFC, originating in the cold air mass, eventually overwhelms the parent cyclone (P). In general, the model reproduces well the genesis, track, and intensity of the frontal cyclone family, their associated thermal structure and precipitation pattern, as well as their surface circulations, as verified against the Canadian Meteorological Centre (CMC) analysis and other available observations; see Part I for more details. We have shown that the frontal cyclones have a depth of 100–300 hPa in the lower troposphere, diameters ranging from 500 to 1100 km (as denoted by the last closed isobar), and a spacing of 1000–1400 km apart (between the circulation centers). They tend to accelerate and experience their central pressure drops, but not necessarily their circulation intensity, as they move from high to low pressure regions (i.e., toward the circulation center of the parent cyclone), and then they decelerate and fill their central pressures as they move away from the parent cyclone. These scaling and deepening characteristics are seen to differ from those large-scale extratropical cyclones as previously studied (see the reviews in Newton and Holopainen 1990).

The purposes of the present study are to (i) document the effects of various physical processes on the frontal cyclogenesis and (ii) examine the relative importance of different dynamical processes in the development of the frontal cyclone family. They will be done by determining the sensitivity of the frontal cyclone family to varying physical parameters at different stages of the cyclones' life cycles and by calculating the vorticity budget using the model-derived datasets. Specifically, we have seen in Part I that the present frontal cyclogenesis occurs in the presence of diabatic heating, the lower-level thermal advection, a warm ocean surface with weak static stability in the maritime boundary layer, a midlevel short-wave trough, a ring of high potential vorticity (PV) near the tropopause, and their mutual interactions. Hence, in this study we will focus on the sensitivity of the model-simulated frontal cyclones to diabatic heating, surface fluxes, surface characteristics, and grid resolution. As part of the understanding, we will also compare the sensitivity results to those that occurred in large-scale cyclogenesis cases, and identify the necessary ingredients for a successful simulation of the storm through the diagnosis of the impacts of various dynamical and physical processes on the simulated track and intensity of the frontal cyclones.

The next section describes the design of sensitivity experiments. Section 3 shows the model sensitivity to

TABLE 1. Summary of sensitivity simulations, the average *e*-folding time (t_e) of the MFC, and the minimum central pressures (P_{min}) of the MFC/NFC.

Code	P_{min} (hPa)	t_e (h)	Remarks
CTL	972/987	21.8	Control simulation
DRY	986/984	40.8	No convective and grid-scale diabatic heating is allowed
G90	987/985	42.5	Dry run with a uniform grid size of 90 km
NOC	994/987	58.2	Dry run with the ocean replaced by a ''land'' surface
NFXD	987/981	43.0	Dry run without surface sensible and latent heat fluxes
NFXM	992/983	52.0	Moist run without surface sensible and latent heat fluxes

latent heat release, and surface sensible and latent heat fluxes from the ocean as well as surface characteristics in the absence of latent heating. Relative importance of the lower-level thermal advection versus the quasigeostrophic forcing will be quantified using the simplified Zwack–Okossi (1986) development equation. Section 4 examines the effects of the surface fluxes in the presence of latent heating on the frontal cyclogenesis. A summary and concluding remarks are given in the final section.

2. Experiment design

To help isolate the relative importance of different processes in the frontal cyclogenesis, five 48-h sensitivity simulations are carried out by turning off a particular parameter in the model while holding all other conditions identical to either a moist or a dry control run. Because of its dominant circulations, our analysis that follows will focus primarily on the genesis and structures of the MFC. Table 1 summarizes all the sensitivity experiments, including the maximum intensity of the MFC and NFC and the nine-point average *e*-folding time (T_e) for the MFC during the final 36-h integration. The *e*-folding time is computed from the modeled quasigeostrophic absolute vorticity (η_g) at the cyclone center in the lowest 100 hPa; that is, $t_e = -(\nabla \cdot \mathbf{V})^{-1} = \Delta t\{\ln[\eta_g(t_1)/\eta_g(t_0)]\}^{-1}$, where $\Delta t = t_1 - t_0 = 6$ h. Note that only one sensitivity simulation, that is, experiment MFXM, includes diabatic heating, which is performed to study the role of surface fluxes in the presence of latent heat release in the frontal cyclogenesis, whereas all the others are conducted by turning off both convective and grid-scale latent heating. Recognizing the nonlinear interactions among all the parameters being examined, their relative contributions to the frontal cyclogenesis can only be assessed between the specific sensitivity and its control runs. Detailed procedures are described as follows.

(i) *No latent heat release* (expt DRY). As shown in Part I, the rapid spinup of the MFC and other frontal cyclones after 14/00–24 is accompanied by intense precipitation, for example, at a rate of >5 mm h^{-1}, near its circulation center. This indicates that latent heating must have played an important role in the deepening of the systems, as has also been shown by many of the previous modeling studies of large-scale extratropic cyclones (e.g., Danard 1964; Anthes and Keyser 1979; Kuo et al. 1991). Thus, it is desirable to quantify the relative significance of latent heating versus dry dynamics in the secondary cyclogenesis. For this purpose, a dry simulation is conducted, in which neither convective nor grid-scale condensation is included (expt DRY). The continuity equation for specific humidity is still integrated in order to include the virtual temperature effect and keep the initial mass field the same as that in experiment CTL. Supersaturation is removed as precipitation falling to the ground, but the feedback of the resulting latent heat to the thermodynamic equation is neglected (see Zhang 1989). Without the condensational heating, the model atmospheric circulations are only determined by advective processes. Therefore, a comparison between experiments DRY and CTL would show how these secondary cyclogenesis events depend on latent heating versus large-scale adiabatic processes.

(ii) *No surface sensible and latent heat fluxes with* (expt NFXM) *or without latent heating* (expt NFXD). Surface heat and moisture fluxes can substantially alter a cyclogenetic environment by reducing its static stability, enhancing condensational heating, and modifying the low-level baroclinicity. In particular, the theoretical studies of Orlanski (1986), Nakamura (1988), and Mak (1998) have emphasized the importance of surface fluxes in mesocyclogenesis even in the absence of latent heating. However, previous numerical studies showed various degrees of their influence on (large scale) cyclogenesis, for example, from having an important positive impact (Kuo et al. 1991; Lapenta and Seaman 1992) to virtually no effect (Petterssen et al. 1962; Reed and Simmons 1991) and a negative impact (Kuo and Low-Nam 1990). Moreover, in a numerical investigation of secondary cyclogenesis, Mailhot and Chouinard (1989) found that the model is unable to reproduce the secondary cyclone and its associated precipitation in the absence of evaporation from ocean. Since the frontal cyclone family under study intensifies in the vicinity of the Gulf Stream, large upward surface fluxes from the warm ocean may be expected to have a substantial impact on the storm's deepening. In view of the different roles of dry and moist dynamics in cyclogenesis, therefore, two sensitivity experiments are performed: one with the surface fluxes switched off from *experiment DRY* so that their influence on the dry cyclogenesis can be evaluated (expt NFXD), and the other with the sur-

face fluxes withheld from *experiment CTL* since surface fluxes are often shown to be more significant in the presence of latent heating (expt NFXM).

(iii) *No oceanic surface characteristics* (expt NOC). Surface characteristics can affect cyclogenesis through the availability of surface moisture for evaporation, which varies from 0 for a dry surface to 1 for a moist surface and, most importantly, through the surface roughness that determines the frictional dissipation of low-level horizontal momentum and the cyclonic spindown by the friction-induced secondary circulations (Holton 1992). In fact, the surface frictional effects have been shown by Mullen and Baumhefner (1989), Huo et al. (1996), and others to be extremely pronounced for explosively deepening (large scale) oceanic cyclones. On the other hand, Mullen (1982) found many similarities of secondary cyclogenesis events that occurred between ocean and continent, suggesting that the surface friction is not essential for secondary cyclogenesis. Since the family of frontal cyclones in the present case deepens over the ocean surface (see Part I), it is of interest to examine whether or not these developments are solely of an oceanic nature. If not, what is its influence on the final intensity of the storm? This could be done by performing a sensitivity experiment, in which the surface roughness length over the ocean is treated as that of ''land'' with a value typical for the continental interior (expt NOC). It should be noted, however, that such an experiment does not isolate completely the frictional effect since the surface winds, modified by the changes in the roughness, will in turn affect the heat and moisture transfers at the ocean surface.

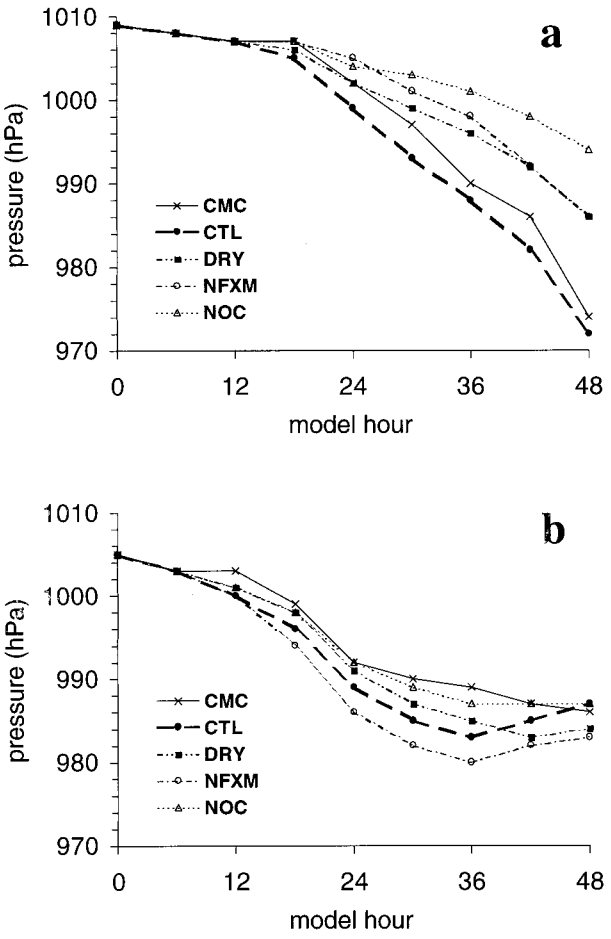

FIG. 2. Time series of the central sea level pressure of (a) the MFC and (b) the NFC from the CMC analysis (solid), CTL (solid circle), DRY (solid square), NFXM (open circle), and NOC (open triangle).

3. Adiabatic simulations

In this section, we discuss only the experimental simulations that exclude latent heating and examine the roles of different dry dynamical processes in the frontal cyclogenesis. In this case, the model dynamics will be similar to the previous theoretical studies of frontal cyclogenesis, for example, Moore and Peltier (1987), Joly and Thorpe (1990), Thorncroft and Hoskins (1990), and Schär and Davies (1990) except for their neglect of surface energy fluxes and surface friction.

a. Influence of diabatic heating versus adiabatic processes

When latent heating is turned off (expt DRY), the structure and intensity of the MFC during the first 18-h integration are nearly the same as that in experiment CTL (see Figs. 1–3), since little precipitation occurs prior to the genesis stage. Then, the MFC deepens at a rate of 2 hPa/3 h, as compared to the control-simulated 3.4 hPa/3 h rate. At the end of the 48-h simulation, the dry MFC is about 14 hPa weaker than the moist one (see Fig. 2), which represents approximately 59% of the total deepening by dry dynamics. In terms of the average *e*-folding time, however, the dry MFC time is 40.8 h, which is about twice as long as that for the moist MFC (see Table 1) and from the aforementioned (dry) theoretical studies. Such a large difference in the *e*-folding time from the theoretical studies suggests that the surface friction plays an important role in slowing the deepening of the frontal cyclones owing to their shallowness in vertical circulations (see Fig. 4). This could be further inferred from the sensitivity simulation NOC to be presented in the next subsection. As discussed in Part I, the similar *e*-folding time between the full physics control run (21.8 h) and the previous (dry) theoretical models (24 h) is attributable to the fact that the dissipative effect of surface friction tends to be offset by the amplifying impact of latent heating. Thus, to obtain a more realistic estimate of the growth rate of frontal cyclones, theoretical studies have to include the effects of both the diabatic heating and the surface friction.

While latent heating plays an important role in the rapid deepening of the MFC, its impact on the track of the system is small (see Fig. 1 in Part I), since it is more or less determined by a ring of PV anomaly in the upper

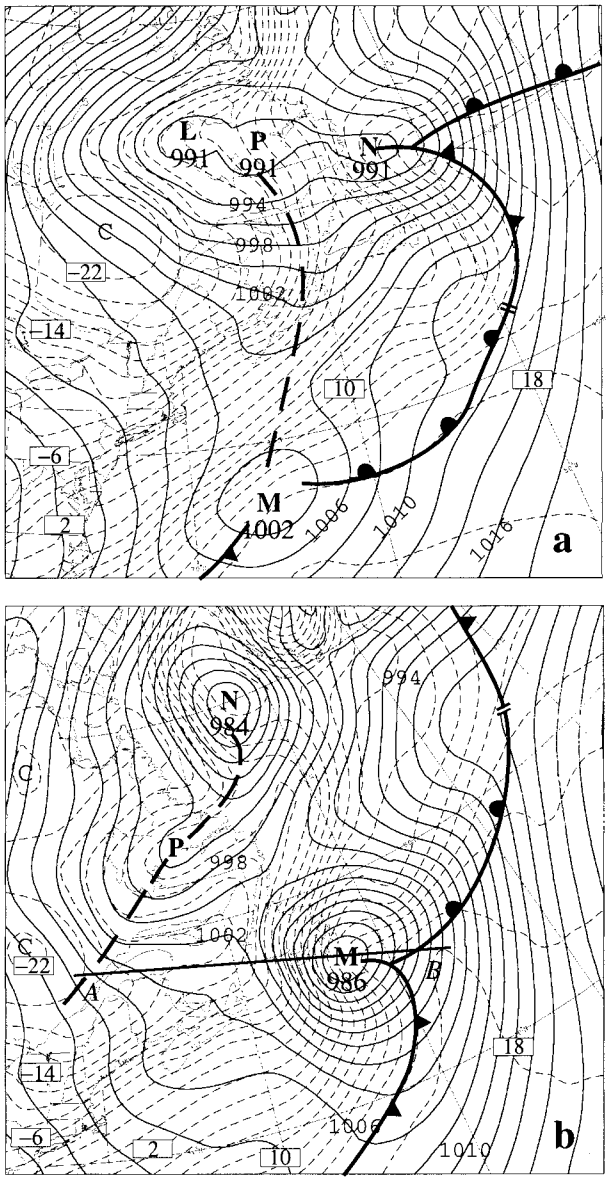

FIG. 3. As in Fig. 1 but for expt DRY (no latent heat release).

troposphere. In addition, the horizontal extent and overall circulation characteristics, including the associated warm–cold frontal structures and the pressure ridge to the north, are similar between the two runs, except for the stronger pressure gradients in the vicinity of the moist MFC (cf. Figs. 1 and 3). However, the dry cyclone moves much slower than the moist one; the difference in position is about 400 km at the end of the 48-h integration (cf. Figs. 1 and 3). This difference in speed results likely from the interaction of the two different MFCs with the similar larger-scale steering flow. That is, in a highly sheared environment a deeper and stronger cyclone tends to be advected more by flows at higher levels. Thus, *the slow movement of the dry MFC is caused by its shallow circulation* (cf. Figs. 4a,b) *interacting with a lower-level weak mean flow.* The above results are in agreement with the previous studies of explosively deepening (large scale) oceanic storms that occurred at much larger scales, for example, Anthes et al. (1983), Chen et al. (1983), Kuo et al. (1991), and Huo et al. (1996). But they are in significant contrast with the coastal cyclogenesis studies by Lapenta and Seaman (1992) and Doyle and Warner (1993), who showed that the cyclogenesis fails to occur in the absence of latent heating.

It should be mentioned that when a grid size of 90 km is used to simulate the case without diabatic heating (expt G90), the model could still duplicate reasonably well the basic structures of the cyclone family, except that the central pressure of the MFC is 1 hPa weaker than that in experiment DRY. This indicates that any grid size between 30 and 90 km is suitable for simulating the energy growth at the frontal-cyclone scale. A fine-grid size of 30 km is used in the moist runs (i.e., expts CTL and NFXM) because it allows the use of the state-of-the-art Kain–Fritsch (1993) cumulus parameterization and grid-scale cloud microphysics schemes.

On the other hand, the slower movement and the weakening of the dry MFC allow the NFC to increase its intensity, that is, by 3 hPa at the end of the 48-h integration (cf. Figs. 1b and 3b). This appears to result from the vortex–vortex interaction when the two cyclones are in close proximity. Specifically, the more intense MFC in experiment CTL tends to produce a stronger pressure ridge and its associated easterly cross-isobaric flows to the north than that in expt DRY. Since the flows between the MFC and NFC are the consequence of superposition of their circulations, the stronger easterly flows associated with the MFC tend to exert a torque opposite to the cyclonic flows of the NFC. Thus, we may expect the NFC to intensify further if the MFC were absent. Such a vortex–vortex interaction could also be seen from the more pronounced southward transport of colder air and stronger surface thermal gradients across the MFC (e.g., 34°C/20° longitude in expt DRY vs 20°C/20° longitude in expt CTL) as a result of the development of the stronger NFC (cf. Figs. 1b and 3b). This appears to explain why the dry MFC deepens more rapidly in the final 12-h integration; its rate is close to that in experiment CTL (Fig. 2a). It should be pointed out that while the NFC is 2 hPa deeper in central pressure than the MFC, its circulation intensity, horizontal extent, and vertical depth are not as robust as the MFC; similarly for the rest of sensitivity simulations presented in this study. This is because the NFC's central pressure drop is largely caused by its movement from a high to lower-pressure region toward the center of the weakening parent cyclone, as discussed in Part I.

Although dry dynamics is able to account for the generation of both the MFC and NFC, the model is unable to generate the SFC with closed isobars in the absence of latent heating; only a weak mesotrough develops (see Fig. 3b). This implies that dry dynamics

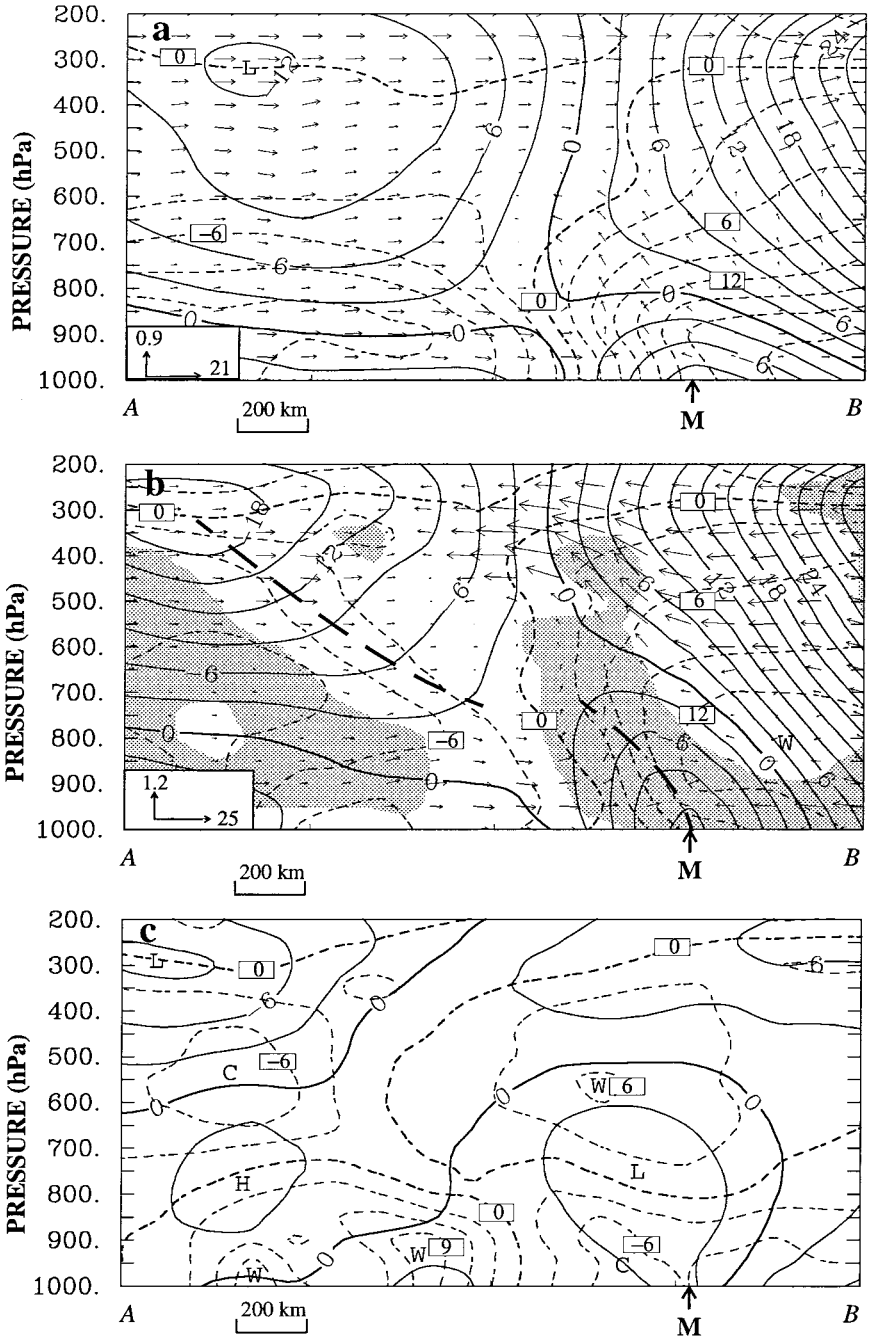

FIG. 4. Vertical cross section of height deviations (solid, every 3 dam) and temperature deviations (dashed, every 3°C), superposed with alongplane flow vectors, which is taken along line AB in Fig. 3b from 48-h integration of (a) expt DRY and (b) expt CTL. Shadings in (b) denote relative humidity $> 90\%$; (c) the differenced height (solid, every 3 dam) and differenced temperature (dashed, every 3°C) between expts CTL and DRY (i.e., CTL along line AB in Fig. 1 minus DRY along line AB in Fig. 3). Inset shows the scale of vertical (Pa s^{-1}) and horizontal (m s^{-1}) motions. Location of the MFC is indicated on the abscissa.

could induce a pressure perturbation associated with the SFC but latent heat energy is needed to transform it into an intense frontal cyclone. This is consistent with the development of a mesoscale cloud system associated with the SFC, as shown in Part I (Fig. 12b therein). Furthermore, the slower propagation of the MFC may suppress the development of the SFC, based on the above-mentioned vortex–vortex interaction argument.

To gain further insight into the relative significance of the diabatic heating versus adiabatic processes in the MFC genesis, we compare the vertical structures of height and temperature deviations between the dry and moist runs and examine their differences at the end of the 48-h integration (see Fig. 4). (The height and temperature deviations are obtained by subtracting their pressure-level averages within the cross section.) A comparison between the dry and moist runs (cf. Figs. 4a,b) reveals (i) the appearance of a much shallower height trough (up to 850 hPa) associated with the weaker (dry) MFC; (ii) the less influence of the dry MFC on the midtropospheric thermal field, as evidenced by the eastward tilt of isotherms above 800 hPa; (iii) the presence of stronger thermal gradients below 800 hPa in the absence of latent heating; and (iv) *the limited depth in the lower half of the troposphere even in the presence of intense latent heating.*

The net (direct and indirect) effects of latent heating on the MFC genesis can be evaluated from Fig. 4c, which displays the height and temperature differences between the two simulations (i.e., CTL minus DRY). In the presence of latent heating, the MFC experiences net warming above 800 hPa with a maximum value of >6°C occurring near 550 hPa and net cooling below with a minimum value of <-6°C. This net warming–cooling profile is hydrostatically consistent with the height deficit (surplus) in the lower (upper) levels. The largest mass deficit difference occurs in the 800–700-hPa layer, that is, just above the shallow circulation of the dry MFC. The lower- (upper-) level net height deficit (surplus) implies increased mass convergence (divergence) in the lower (upper) troposphere, which is favorable for deeper cyclonic development; the opposite is true for the parent cyclone to the left.

Figure 4c also depicts the influence of the interaction between the MFC and NFC on the low-level thermal field. The lowest 200 hPa in the CTL cold sector, that is, to the west of the MFC, is more than 9°C warmer than that in experiment DRY (cf. Figs. 1b, 3b and 4c) as a result of the enhanced cold advection associated with the (dry) NFC. By comparison, above 800 hPa in the cold sector, pronounced cooling occurs as more cold air mass is transported into the region by the enhanced (MFC) cyclonic circulations in experiment CTL relative to its dry counterparts, which is hydrostatically consistent with the net height deficit above and surplus below. This further reveals that the development of the frontal cyclones tend to accelerate the dissipation of the parent cyclone at the lower levels.

The low-level vorticity structure from the 24-h dry run is given in Fig. 5a, which shows several elongated cyclonic circulations superposed along the leading frontal zone. Two of the distinct vorticity centers, consisting primarily of shear vorticity, are associated with the MFC and NFC. After the 6-h spinup (see Fig. 2), the MFC's relative vorticity exceeds the local Coriolis parameter. A vertical cross section of the relative vorticity shows

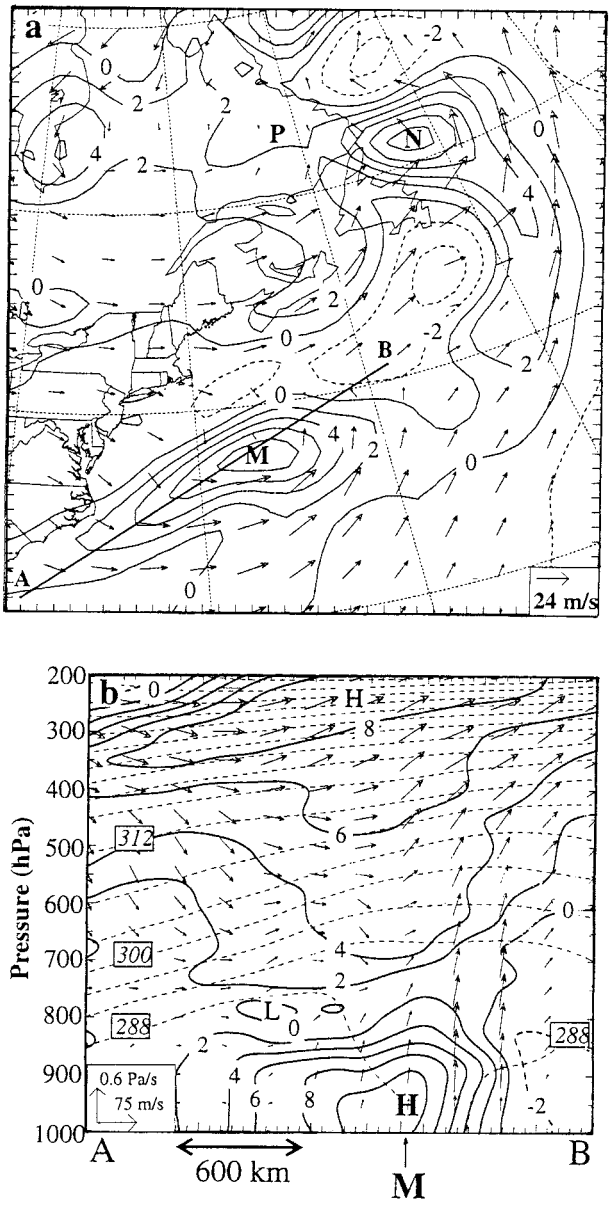

FIG. 5. (a) Horizontal distribution of 950-hPa relative vorticity at intervals of 2×10^{-5} s^{-1}, and (b) vertical cross section of relative vorticity (solid) at intervals of 2×10^{-5} s^{-1} and potential temperature (dashed) at intervals of 4 K, taken along line AB in (a); both from 24-h integration of expt DRY.

again that the MFC is a shallow system with its circulation up to 800 hPa (cf. Figs. 4a and 5b). More importantly, the MFC intensifies in a near-neutral boundary layer below 750 hPa due to the presence of an underlying warm ocean surface, as can also be seen from a vertical sounding taken at the MFC center in Part I (Fig. 7a). (Note that the weak thermal gradient seen in Fig. 5b compared to that in Fig. 3 is due to the orientation of the vertical cross section that is taken nearly parallel to the low-level isotherms.) Of further importance is the presence of a deep layer of upper-

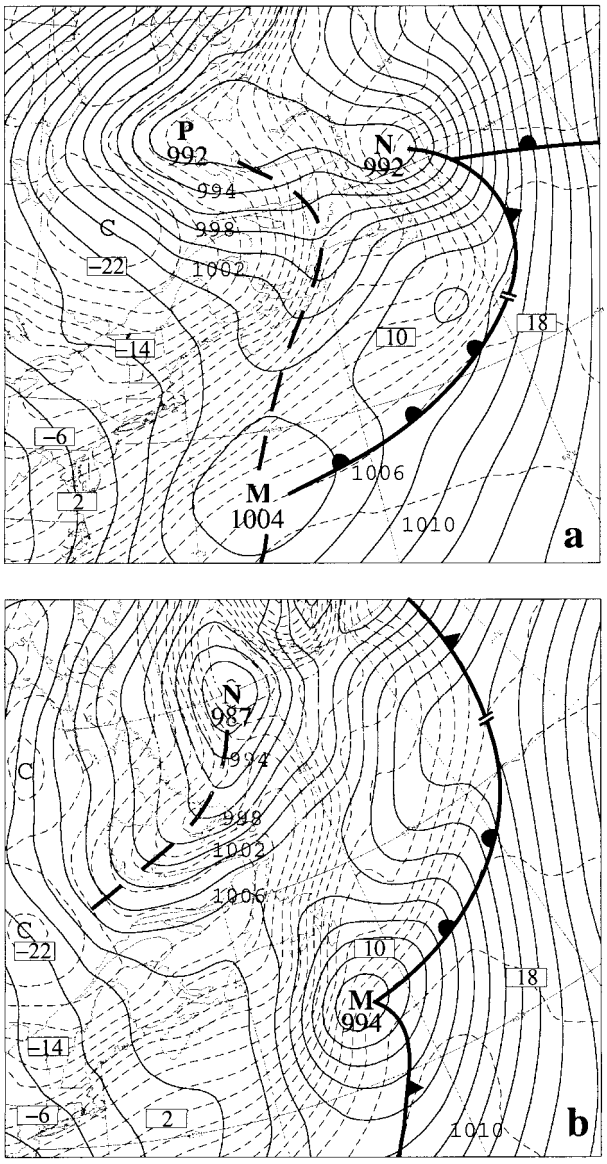

FIG. 6. As in Fig. 1 but for expt NOC (no ocean surface characteristics).

level cyclonic vorticity (with a maximum of $>8 \times 10^{-5}$ s^{-1} at 250 hPa) that descends in the westerly flow toward the MFC. This is distinct from the lower-level cyclonic vorticity associated with the MFC that spins up through vortex stretching in the ascending flow. As has been shown in Part I (see Figs. 3b and 14b therein), this descending vorticity is related to a ring of positive PV with the stratospheric origin on the cyclonic side of an upper-level jet streak; its core is tilted northward with height. This suggests that the upper-level vorticity advection associated with the PV ring must play an important role, at least, during the genesis stage of the MFC, as will be further shown in section 3c.

b. Influence of ocean surface characteristics

Since both the MFC and NFC can develop in the absence of latent heating, it is natural to examine whether or not the dry frontal cyclogenesis is mainly caused by the relatively smooth ocean surface. Surprisingly, the model is still able to generate the MFC and NFC when the ocean surface in experiment DRY is replaced by a ''continental'' surface (expt NOC). The basic circulation structures resemble closely their pure dry counterparts (cf. Figs. 3 and 6). This further enforces the conclusion that dry dynamics plays an essential role in the present secondary cyclogenesis events. However, treating the ocean as land results in the development of the weakest and slowest-moving MFC among all the sensitivity tests performed, similarly for the NFC (see Fig. 2 and Table 1). For example, the MFC in experiment NOC at the end of the 48-h integration is 8 (22) hPa weaker and 500 (1100) km slower than that in experiment DRY (CTL) (see Fig. 3). The average *e*-folding time is 58.2 h (see Table 1), which is much longer than that in experiments DRY (40.8 h) and CTL (21.8 h). As will be shown in the next section, the impacts of ocean surface sensible and latent heat fluxes on the cyclogenesis with and without latent heating are small. Hence, the 8-hPa pressure difference between experiments DRY and NOC is caused primarily by the difference in surface drags. This result is qualitatively consistent with the Ekman-layer theory in which the *e*-folding time (τ) of cyclonic spindown is proportional to the depth of cyclonic circulations (H) and inversely proportional to the square root of eddy viscosity (K_m), that is, $\tau \equiv \sqrt{2}H(fK_m)^{-1/2}$, where f is the Coriolis parameter (see Holton 1992). Thus, increasing the surface drag will result in a more rapid spindown of cyclonic vorticity through the friction-induced secondary circulations and a more rapid loss of the low-level horizontal momentum. Apparently, this cyclonic spindown is more pronounced for frontal cyclones than their large-scale counterparts because of their shallowness and small-scale nature. It follows that (i) the Ekman spindown is an important parameter in determining the amplification rate of frontal cyclones and it is necessary to incorporate it into theoretical models to obtain a better understanding of frontal cyclogenesis and (ii) the more rapid frontal cyclogenesis phenomena tend to occur more frequently over oceans.

Note again that the NFC is deeper than the MFC in terms of central pressure, but the opposite is true for its circulation intensity (Fig. 6a,b). As in experiment DRY, the central pressure depends partly on the distance relative to the parent cyclone center, whereas the circulation intensity is determined by dynamical forcings and diabatic heating. As discussed in Part I, this represents one of the basic characteristics that differs from the large-scale cyclogenesis.

c. Relative importance of upper- versus low-level adiabatic processes

Since dry dynamics accounts for the genesis and a large portion of the total deepening of the MFC and NFC, it is necessary to examine the relative contributions of different dynamic processes to the frontal cyclogenesis. In fact, one of the FASTEX objectives is to understand the contributions of upper- and lower-tropospheric processes to frontal cyclogenesis (Snyder 1996). For this purpose, we choose to use the simplified Zwack–Okossi (1986) development equation (Lupo et al. 1992, henceforth Z–O) and apply it to the dry simulation. The Z–O equation provides a complete description of all the forcing contributions at any level to the geostrophic vorticity changes at the surface or any pressure level close to the surface. In the present case, the vorticity budget is performed at 950 hPa, at which level the frictional effect is considered small and so it can be neglected. The modified Z–O equation given in Lupo et al. (1992), after neglecting diabatic heating and friction, can be simplied further as follows:

$$\frac{\partial \zeta_{gl}}{\partial t} = P_d \int_{P_t}^{P_l} (-\mathbf{V}\cdot\boldsymbol{\nabla}\zeta_a)\, dp - P_d \int_{P_t}^{P_l} \left[\frac{R}{f}\int_{P_t}^{P_l} \nabla^2(-\mathbf{V}\cdot\boldsymbol{\nabla}T + S\omega)\frac{dp}{p}\right] dp, \quad (1)$$

where ζ_{gl} is the geostrophic vorticity, $P_l = 950$ hPa, $P_t = 100$ hPa, and $P_d = (P_l - P_t)^{-1}$, $\zeta_a\ (=\zeta + f)$ denotes the absolute vorticity, S is the static stability parameter defined as $S = -(T/\theta)(\partial\theta/\partial p)$, and the other variables have their conventional meaning. The vertical velocity, ω, in p coordinates is calculated using the omega equation as derived by Tsou and Smith (1990):

$$\left[\frac{R}{p}S\nabla^2 + f(\zeta + f)\frac{\partial^2}{\partial p^2}\right]\omega = -f\frac{\partial}{\partial p}(-\mathbf{V}\cdot\boldsymbol{\nabla}\zeta_a) - \frac{R}{p}\nabla^2(-\mathbf{V}\cdot\boldsymbol{\nabla}T). \quad (2)$$

Equation (2) implies that the vertical motion consists of the contributions due to vertical differential vorticity advection (ω_ζ) and the Laplacian of thermal advection (ω_T). The combination of Eqs. (1) and (2) gives the final form of the Z–O vorticity budget used in our analysis of the dry simulation:

$$\frac{\partial \zeta_{gl}}{\partial t} = P_d \int_{P_t}^{P_l} \left[-\mathbf{V}\cdot\boldsymbol{\nabla}\zeta_a - \frac{R}{f}\int_{P}^{P_l} \nabla^2(S\omega_\zeta)\frac{dp}{p}\right] dp - P_d \int_{P_t}^{P_l} \left[\frac{R}{f}\int_{P}^{P_l} \nabla^2(-\mathbf{V}\cdot\boldsymbol{\nabla}T + S\omega_T)\frac{dp}{p}\right] dp. \quad (3)$$

Terms on the right-hand side of Eq. (3) represent the column-integrated contributions due to the vertical differential vorticity advection and the Laplacian of horizontal temperature advection to the net vorticity tendency at 950 hPa. Both terms include a purely advective part and vorticity changes due to the adiabatic cooling (warming) in their induced ascent (descent). It is found that the induced cooling or warming effects are always negatively correlated with but weaker than their advective contributions (not shown).

Figure 7 shows one example of the column-integrated vorticity budget from the 24-h dry simulation, at which time the MFC just forms its first closed isobar. Two well-organized positive–negative tendency couplets are seen corresponding to the MFC and NFC, with their centers located near the null tendency isopleths (Fig. 7c). The positive tendency centers represent roughly the locations where the cyclones are about to propagate, and thus Eq. (3) predicts correctly the movement and the trend of cyclonic development. Because the NFC has entered its most rapid deepening stage by this hour, its vorticity tendency couplet is greater in both amplitude and horizontal extent than the one associated with the MFC.

The net vorticity tendency couplets are well coordinated with the column-integrated contributions due to the vorticity advection and the Laplacian of thermal advection, with very slight phase shifts (cf. Figs. 7a–c). The vorticity contributions are closely related to the propagation of low-level cyclonic vorticity *that intensifies with time* and the advection of upper-level cyclonic vorticity associated with the PV ring *that changes little during the life cycle of the MFC* (Fig. 5), whereas the thermal contributions occur primarily at the lower levels, being positive (negative) ahead (behind) in the southeasterly (northwesterly) sloping flow along the warm- (cold-) frontal zones (see Fig. 7c). [It should be mentioned that moderate upper-level thermal advection occurs only behind trough T_1 and ahead of the large-scale jet stream (see Figs. 3 and 14 in Part I), which do not seem to have any significant impact on the MFC genesis.] It is evident that both forcings exhibit well-defined positive contributions to the cyclonic developments. Of importance is that the thermal contributions to the column-integrated net tendencies are greater than those due to the vorticity advection for both the MFC and NFC. This suggests that the lower-level thermal advection plays an important role in the genesis of the MFC and NFC, since more significant thermal advection occurs in the lowest 300 hPa (see Fig. 4) where both the flows (>20 m s^{-1}) and thermal gradients (2°–4°C/100 km) are intense.

To help understand the relative significance of the differential vorticity advection and the Laplacian of (low level) thermal advection during different stages of the MFC and NFC, Tables 2 and 3 show the 12-hourly area-averaged contributions to the net vorticity tendency at 950 hPa. It can be seen from Table 2 that the magnitudes of both advective effects increase with time, which is consistent with the continued deepening of the MFC.

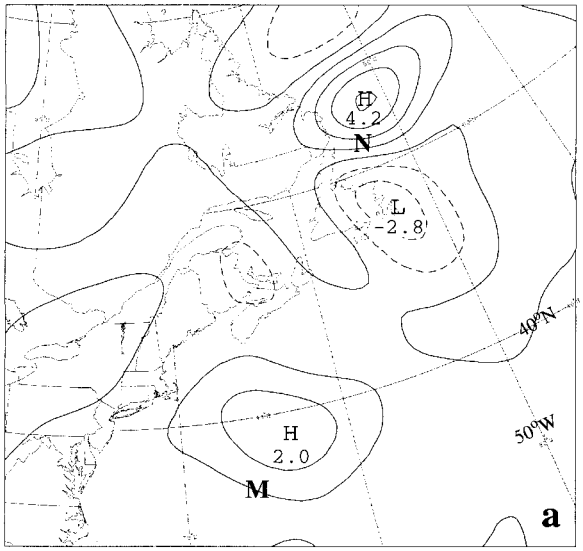

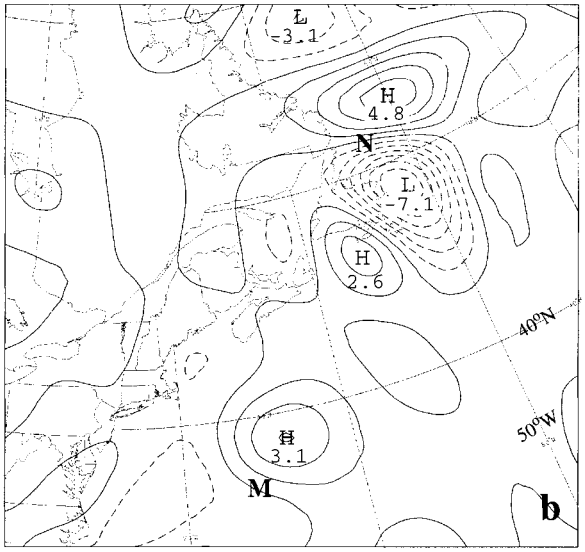

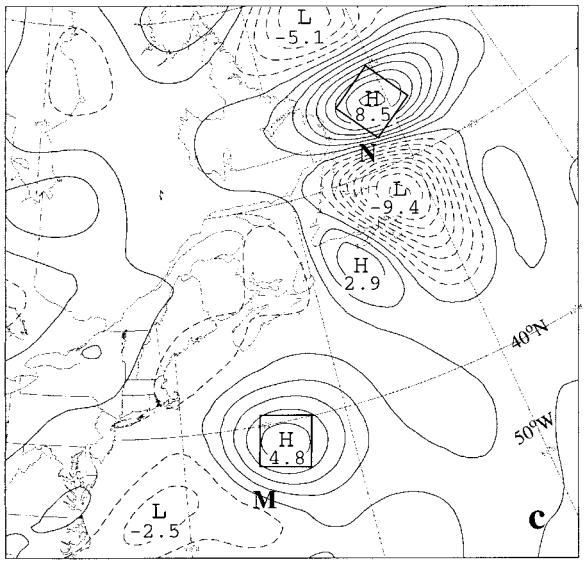

TABLE 2. The magnitudes (10^{-9} s^{-2}) and relative contribution (%) of the column-integrated differential vorticity advection and the Laplacian of the thermal advection to the net geostrophic vorticity tendency at 950 hPa that are averaged over an area of 270 km × 270 km ahead of the MFC center (see Fig. 7c).

	13/12–12	14/00–24	14/12–36	15/00–48
Vorticity (%)	0.9 (36)	2.0 (37)	3.6 (38)	5.2 (41)
Thermal (%)	1.5 (64)	3.1 (63)	5.8 (62)	7.6 (59)

Of interest is that despite the concurrent increases, their relative importance remains nearly steady during the life cycle of the MFC, namely, the thermal contribution accounts for over 60% of the total (dry) deepening. Note though that this type of budget calculation tends to overestimate the percentage contribution of the vorticity advection, since a large portion of the remaining 40% contribution is associated with the advection of the MFC's low-level cyclonic vorticity. This implies that the intense low-level thermal advection is crucial not only to the genesis, but also to the explosive deepening of the MFC.

Likewise, the magnitudes of thermal and vorticity contributions to the net vorticity tendency of the NFC increase as it enters its mature stage; again their relative importance remains nearly the same, that is, about 50 to 50 (see Table 3). Both contributions decrease after 36 h into the integration owing mainly to the ''blocking'' effect of the Greenland topography, which is consistent with the slow evolution of the NFC.

The above findings appear to differ from the previous studies of large-scale oceanic storms in which the vorticity advection contributes the most to cyclogenesis during the explosive deepening phase (Lupo et al. 1992; Reed et al. 1994; Huo et al. 1996). The lack of pronounced vorticity advection in the upper troposphere appears to explain why the present frontal cyclones remain shallow in vertical circulation compared to their large-scale counterparts in spite of the significant upper-level PV forcing or even in the presence of intense diabatic heating. It should be noted, however, that while the low-level thermal advection dominates the frontal cyclogenesis in the present case, the upper-level PV advection plays an important role in triggering the genesis processes and controlling the movement of the frontal cyclones.

←

FIG. 7. Horizontal maps of the column-integrated vorticity budget at intervals of 10^{-9} s^{-2} at 950 hPa from 24-h integration of expt DRY: (a) contribution of differential vorticity advection, (b) contribution of the Laplacian of temperature advection, and (c) the net tendency. Centers of the MFC and NFC are marked by M and N, respectively. Boxes in (c) indicate the area over which the vorticity tendencies are averaged (see Tables 2 and 3).

TABLE 3. As in Table 2 but for the NFC.

	13/12–12	14/00–24	14/12–36
Vorticity (%)	2.5 (49)	4.2 (47)	4.7 (52)
Thermal (%)	2.6 (51)	4.8 (53)	4.3 (48)

4. Effects of oceanic sensible and latent heat fluxes

When both the latent heating and surface fluxes are turned off (experiment NFXD), the track (not shown) and central pressure trace (Fig. 2) of the MFC follow closely those in experiment DRY (also see Figs. 3 and 8); its central pressure is only 1 hPa weaker than its pure dry counterpart at the end of the 48-h integration. Note, however, that the central pressure difference is relatively larger at the MFC's incipient stage, that is, 3 hPa at 14/00–24 (see Table 4). This 3-hPa pressure difference is mainly caused by the surface sensible heat flux over the warm ocean, since water vapor does not condense and the virtual effect of surface moisture flux is negligible in the absence of latent heating. Specifically, prior to 14/00–24, the upward surface heat flux over the Gulf Stream occurs ahead of the cold front. This tends to increase the across-frontal thermal gradient, at least in the boundary layer (see Fig. 3), thereby assisting the spinup of the MFC in the context of dry dynamics—a positive effect[1] on the frontal cyclogenesis (Orlanski 1986; Nakamura 1988; Mak 1998). As the system moves far offshore, on the other hand, strong upward heat flux takes place primarily in the cold sector, as shown in Fig. 9, thus weakening the thermal gradient across the cold front (cf. Figs. 3 and 8). This explains why the central pressure difference between the two runs decreases toward the end of the 48-h simulation—a negative impact on the frontal cyclogenesis. Apparently, *whether or not the upward surface fluxes would have a positive impact on the frontal cyclogenesis depends on their location relative to the frontal systems.* Nevertheless, the final intensity of the MFC in experiments DRY and NFXD indicates that in the absence of latent heating, the surface heat fluxes have very weak impact, through modifying the low-level baroclinicity, on the evolution and final intensity of the frontal cyclones. Thus, it would be more meaningful to investigate the effects of surface fluxes on the cyclogenesis in the presence of phase changes.

When the surface fluxes are withheld from experiment CTL but latent heating is allowed (expt NFXM), the model captures reasonably well the timing and location of the family of frontal cyclones as well as their life cycles (see Figs. 10a,b). Nevertheless, the central pressure traces exhibit a continuing underdeepening of the MFC compared to that in experiment CTL (see Fig. 2a)—an indication of the positive influence of surface fluxes on the (moist) cyclogenesis. At the end of the 48-h simulation, the MFC is 14 hPa weaker than that in experiment CTL, which indicates that about 59% of the total deepening is due to the surface fluxes. This impact is as pronounced as turning off the latent heating

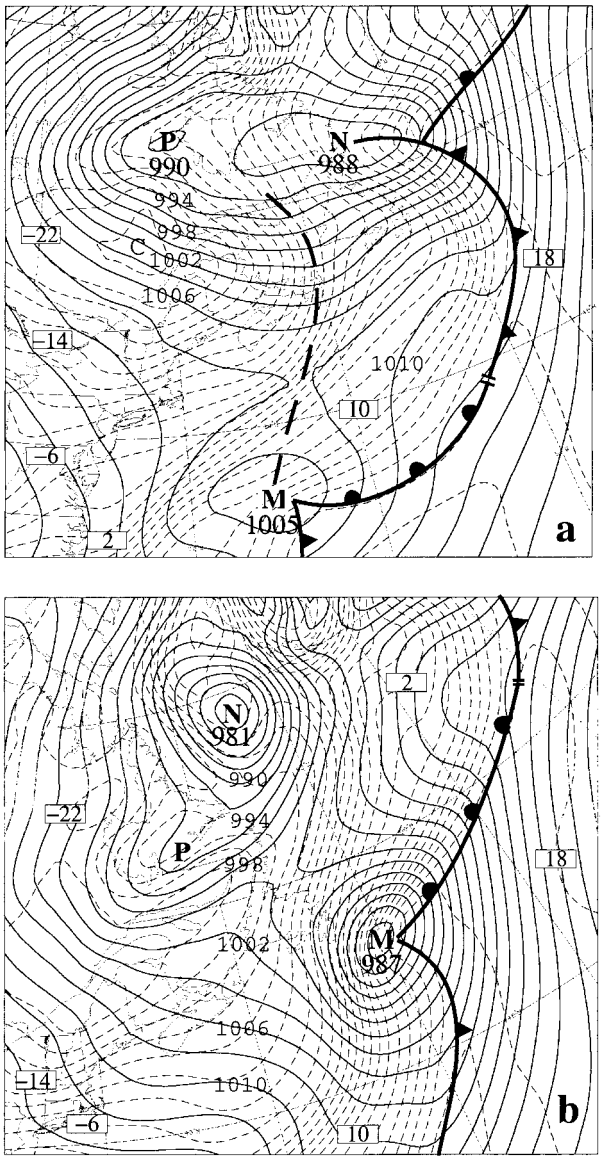

FIG. 8. As in Fig. 1 but for expt NFXD (dry simulation with no surface fluxes).

TABLE 4. Central pressure differences (hPa) between (a) expts NFXD and DRY (DP_{DRY}), and (b) expts NFXM and CTL (DP_{MST}).

	14/00–24	14/12–36	15/00–48
DP_{DRY}	3	2	1
DP_{MST}	6	10	14

[1] In this sense, perhaps it would be more illustrative if the NFXD, NFXM, and control runs are initialized 24 h or more earlier, since the marine boundary layer with weak static stability has already well developed at the model initial time.

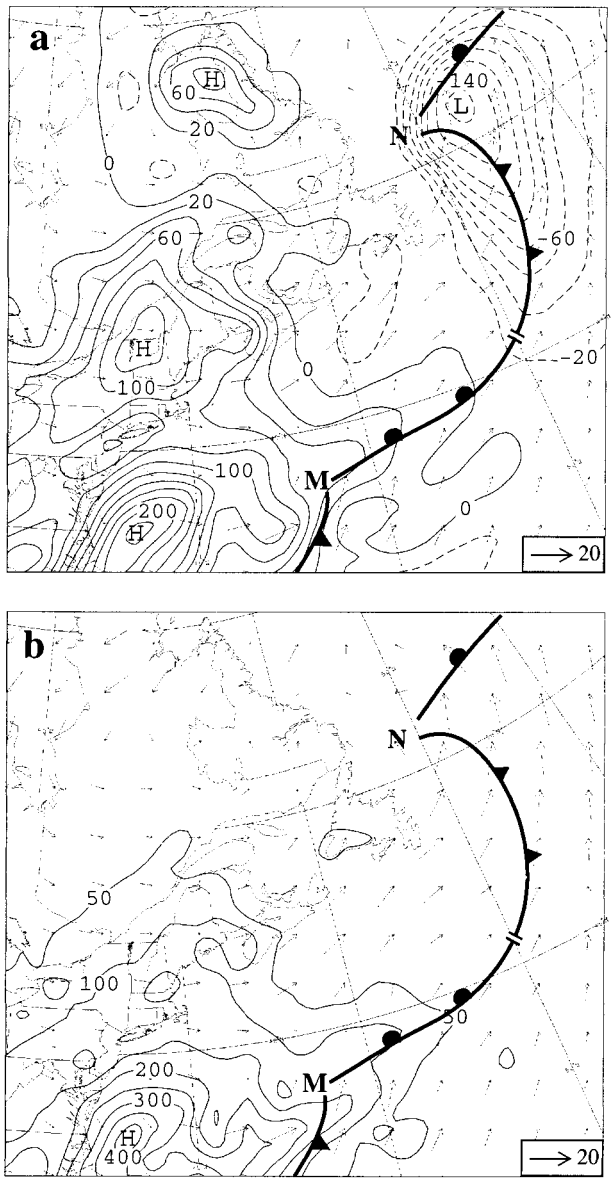

FIG. 9. Distribution of (a) surface sensible heat flux at intervals of 20 W m^{-2} and (b) surface latent heat flux at intervals of 50 W m^{-2}, superposed with 900-hPa wind vectors from 24-h control simulation.

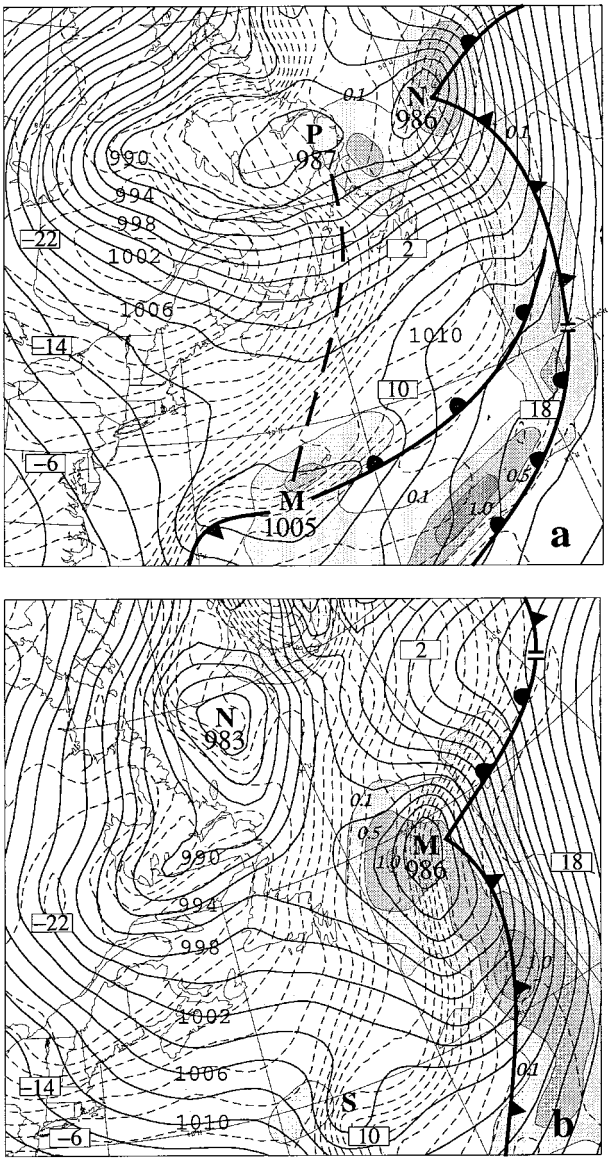

FIG. 10. As in Fig. 1 but for expt NFXM (moist simulation with no surface fluxes). Shading denotes the precipitation rates, contoured at 0.5, 1, 2, and 5 mm h^{-1}.

from the control run! Furthermore, experiment NFXM reproduces the development of the SFC after 36 h into the integration, although it is relatively weak. It follows that the surface fluxes do play a significant role in frontal cyclogenesis in the presence of latent heating, apparently through reducing the static stability (see Fig. 5b) and increasing the moisture content in the warm sector. This can be seen from Fig. 11, which shows a more than 10-K increase of θ_e to the south in the warm sector. The result conforms to the theoretical study of cyclogenesis by Fantini (1991), who found enhanced normal mode growth of oceanic cyclones when pronounced latent heat fluxes occur in the warm sector. Note, though, that *the deepening rate* of the MFC becomes closer to that in experiment CTL after 36-h integration (see Fig. 2a), suggesting that the impact of surface fluxes on the MFC genesis is not significant during the mature stage in the present case. This is attributable to the rapid decreases of surface fluxes in the vicinity of the MFC as it moves northeastward into a colder water surface (see Fig. 1 in Part I and Figs. 9 and 11 herein) where the continuing northward transport of tropical high-θ_e air tends to reverse the air–sea temperature gradient in the warm sector. Otherwise, the central pressure difference between the two runs could be much more pronounced.

Since the surface fluxes affect the cyclogenesis more markedly in the presence of latent heating, it is desirable

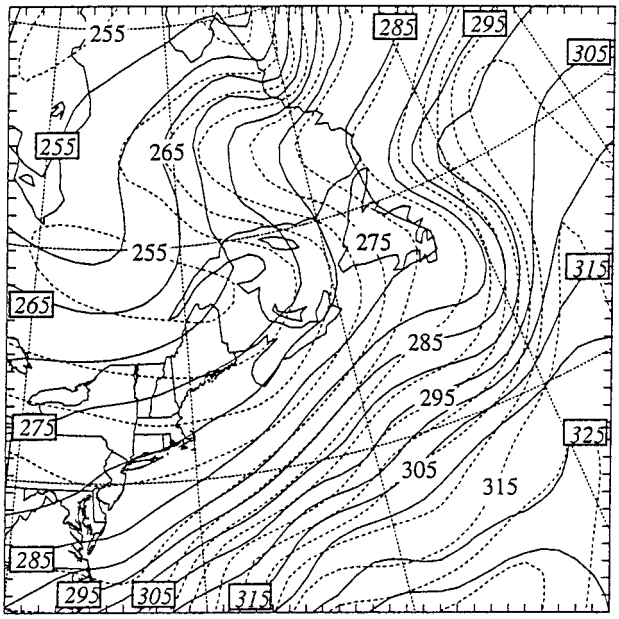

FIG. 11. Distribution of equivalent potential temperature at interval of 5 K from 24-h integrations between expts CTL (solid) and NFXM (dashed).

to compare the 48-h accumulated precipitation between experiments CTL and NFXM in relation to the MFC development. It is evident from Fig. 12a that more precipitation is concentrated along the track followed roughly by all the frontal cyclones (i.e., near their centers) and along the quasi-stationary large-scale cold front. In both runs, stratiform precipitation dominates, which is also typical in rapidly deepening cyclones. In the case of turning off the surface fluxes, significant delay occurs in both the convective and stratiform precipitation (cf. Figs. 12a,b and Figs. 12c,d), and the amount and area coverage are markedly reduced. Moreover, much less (stratiform) precipitation is generated near the center of the MFC prior to 14/18–42 (see Figs. 12b,d). In contrast, more precipitation occurs along the leading warm front as the tropical high-θ_e air overruns the frontal zone (cf. Figs. 10a and 12b). Since this precipitation region is located to the south of the MFC, it tends to intercept convective available potential energy (CAPE) and moisture content that would be otherwise released near the MFC's center, resulting in the diminished efficiency of latent heating at amplifying the cyclone (Hack and Schubert 1986). All this helps explain the slow deepening of the MFC in experiment NFXM up to 14/12–36 (see Fig. 2). Subsequently, the precipitation rate increases, especially near the MFC center, and it becomes more comparable in magnitude to that in experiment CTL near the end of the 48-h integration (cf. Figs. 12a,b). This gives rise to the development of more localized circulations in the vicinity of the MFC (see Fig. 10b).

Of particular interest is that while latent heating is responsible for 59% of the MFC's total deepening in comparing experiments CTL and DRY, it produces little difference in the deepening rate and final depth of the system when surface fluxes are withheld. Only a 1-hPa central pressure difference occurs between experiments NFXM and NFXD at the end of the 48-h integration (cf. Figs. 8b and 10b) in spite of the considerable precipitation occurring in experiment NFXM. The small central pressure difference could be again attributed to the delay in latent heating and the poor efficiency of latent heat release in the vicinity of the MFC, as discussed above.

Another factor that could account for the small pressure difference appears to be closely related to the diabatic influence on the baroclinic structures of the lower troposphere. Specifically, the diabatic heating–cooling modifies significantly the low-level thermal and pressure structures (cf. Figs. 3, 8, and 10). For example, the intense precipitation band to the east of the MFC helps form a new surface frontal zone ahead of the primary ''cold'' front (cf. Figs. 8a, 10a, and 12b). This tends to reduce the advection of warm tropical air into the MFC and forces it to deepen in the cold sector (rather than in the leading frontal zone) for a period longer than that in experiment NFXD (cf. Figs. 8 and 10). The result reveals that the impact of surface fluxes on moist cyclogenesis depends not only on how much precipitation could be produced but also on where the latent heat is released with respect to the cyclone center.

5. Summary and conclusions

In this study, a series of sensitivity experiments is performed, using the simulation presented in Part I as a control run, to study the relative influence of dry dynamics, latent heating, surface friction, surface sensible, and latent heat fluxes on the development of a family of frontal cyclones that occurred over the western Atlantic Ocean. The most important conclusions are summarized below:

- It is found that dry dynamics determines the initiation and track of all the frontal cyclones in the present case, and moist processes help deepen the systems. The movement of the frontal cyclones is determined by their interaction with the large-scale sheared steering flow and their distance with respect to the parent cyclone center. A deeper cyclone tends to move faster than a shallower one in the present positive sheared environment. Dry dynamics accounts for about 59% of the total deepening of the MFC, and its average *e*-folding time (40.8 h) is almost twice as long as that of the moist MFC (21.8 h).
- Vorticity budget calculations reveal that advection of the preexisting upper-level vorticity associated with a PV ring appears to provide the necessary forcing for the initiation and tracking of the frontal cyclones, but *the low-level thermal advection accounts for a larger*

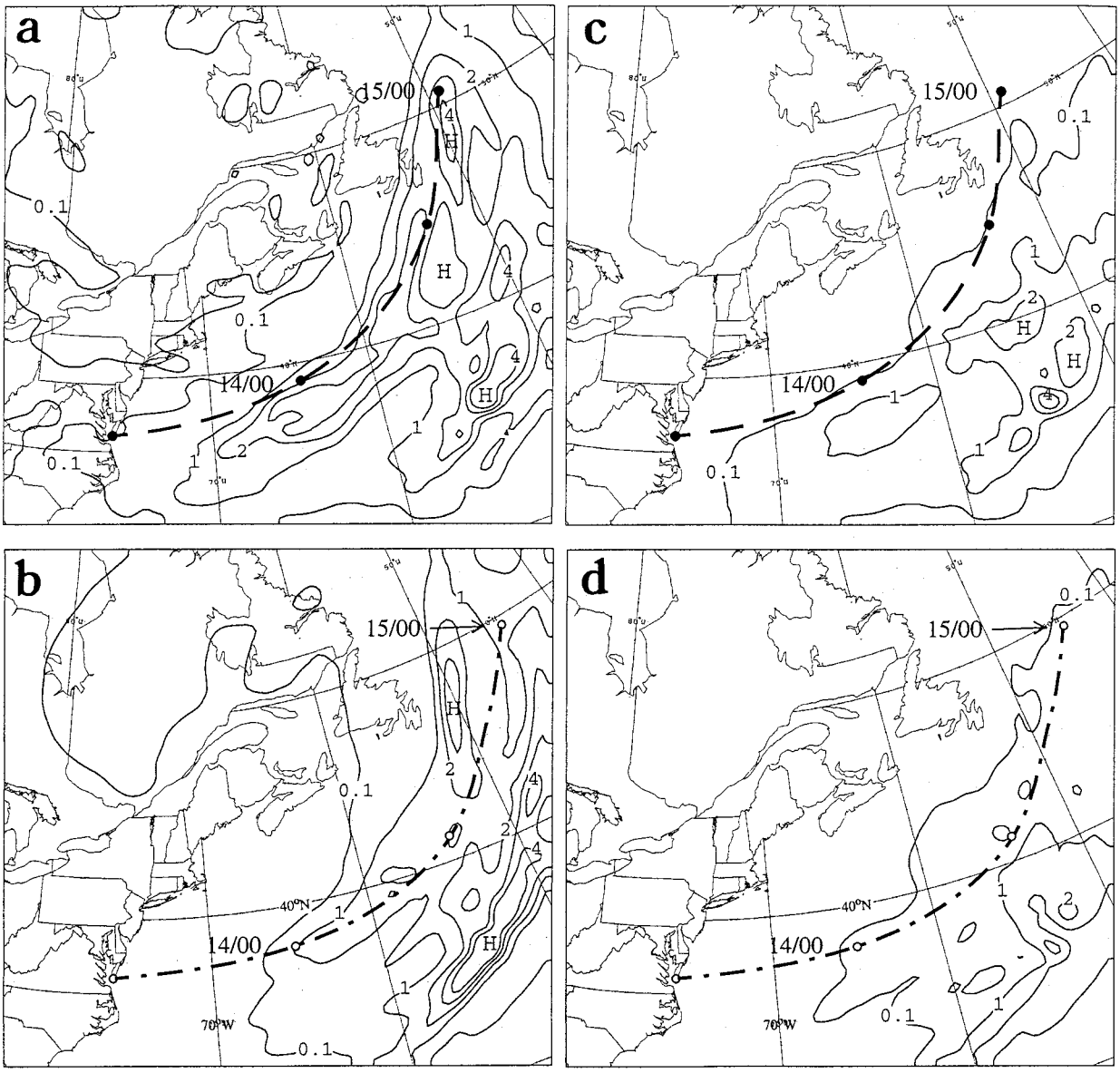

FIG. 12. The 48-h accumulated total precipitation for (a) expt CTL and (b) expt NFXM; and the 48-h accumulated convective precipitation for (c) expt CTL and (d) expt NFXM, with contours at 0.1, 1, 2, 3, and 4 cm. The simulated MFC track is also shown.

portion of the total deepening of the (dry) MFC and NFC. (The effects of the PV ring on the frontal cyclogenesis will be further discussed in a forthcoming paper.) This finding appears to differ from many of the previous studies of larger-scale rapidly deepening cyclones in which upper-level vorticity advection often dominates over the thermal advection in surface cyclogenesis. In particular, *the lack of pronounced upper-level vorticity advection appears to explain why the frontal cyclones tend to remain in the lower troposphere even in the presence of intense diabatic heating.*

- The impact of surface sensible and latent heat fluxes on the frontal cyclogenesis depends on the stages of the cyclones' development and their locations with respect to the warm water surface. Sensitivity results show that in the absence of latent heating, the surface fluxes have very weak impact, through modifying the low-level baroclinicity, on the evolution and final intensity of the frontal cyclones. By comparison, when latent heating is allowed, the surface fluxes make significant differences in the deepening of the frontal cyclones as a result of reduced static stability and increased moisture content in the maritime boundary layer. Without the surface fluxes, the moist simulation produces much less convective precipitation ahead of the primary cold front and delay of grid-box saturation near the cyclone center. In this case, the surface fluxes

accounts for about 59% of the MFC's deepening, which is as pronounced as the latent heating.

- In the absence of the surface fluxes, the moist simulation produces small differences from the dry run in the final intensity of the frontal cyclones. They are attributable to (i) the delay in latent heat release and (ii) the formation of a new frontal zone associated with a precipitation band, which reduces the advection of warm, moist tropical air into the MFC and forces it to deepen in the cold sector (rather than in the leading frontal zone). The results suggest that the impact of surface fluxes on cyclogenesis depends not only on how much precipitation could be produced but also on where the latent energy is released with respect to the cyclone center.
- When the ocean surface is replaced by a typical continental surface characteristics, dry dynamics are still able to produce both the MFC and NFC, although they are the slowest moving and deepening systems among all the sensitivity tests being conducted. The results reveal that (i) *the Ekman spindown is an important parameter in determining the amplification of (shallow) frontal cyclones because the spindown e-folding time is proportional to the depth of cyclonic circulations and inversely proportional to the boundary layer eddy viscosity* and (ii) more rapid frontal cyclogenesis phenomena tend to occur more frequently over a warm ocean surface because of its associated small eddy viscosity and its generated weak static stability.
- Significant vortex–vortex interactions occur within the family of frontal cyclones. It is shown that a slower-moving, weaker MFC tends to reduce its influence on the intensification of the NFC so that the latter attains a lower central pressure even in the absence of latent heating, but it suppresses the development of the SFC. Such interactions also occur in the consumption of available potential energy. That is, most of the latent energy supply from the tropical region tends to be intercepted by precipitating clouds to the south of the systems.

In conclusion, the family of frontal cyclones occurs as a result of the nonlinear interactions among various dynamical and physical processes, such as a ring of upper-level PV anomalies with a short-wave trough approaching to a region of lower static stability, an intense baroclinic zone in the lowest 200 hPa, a warm underlying sea surface, latent heat release near the cyclones' center, and the vortex–vortex interference. No single process can be responsible for the full development of the frontal cyclones. Our results indicate that *theoretical studies have to include the effects of both the diabatic heating and the surface friction in order to obtain a more realistic estimate of the growth rate of frontal cyclones*. Of course, more case studies of frontal cyclone families are needed to generalize the above findings. Considering the great difficulties of many operational models in predicting mesocyclogenesis in polar frontal zones, the above results clearly indicate the importance of obtaining more realistic upper-air observations (e.g., midlevel short-wave disturbances, upper-level jet streaks, and PV anomalies) and sea surface temperatures into operational model initial conditions in hope of improving numerical weather prediction of the phenomena. In this regard, the FASTEX data are providing an important opportunity to examine the predictability of frontal cyclogenesis events and study the mechanism(s) whereby they occur.

Acknowledgments. We are grateful to Lance Bosart for his continuous interest and support and Peter Zwack for providing his vorticity budget program for the present study. We thank Mr. William Cheng for plotting Fig. 5. The computations were performed at the National Center for Atmospheric Research, which is sponsored by the National Science Foundation, under Grant ATM-9413012. This work was supported by Atmospheric Environment Service of Canada and NSF Grant ATM-9802391.

REFERENCES

Anthes, R. A., and D. Keyser, 1979: Tests of a fine-mesh model over Europe and the United States. *Mon. Wea. Rev.,* **107,** 963–984.

——, Y.-H. Kuo, and J. R. Gyakum, 1983: Numerical simulation of a case of explosive marine cyclogenesis. *Mon. Wea. Rev.,* **111,** 1174–1188.

Chen, S.-J., C. B. Chang, and D. J. Perkey, 1983: Numerical study of an AMTEX'75 oceanic cyclone. *Mon. Wea. Rev.,* **111,** 1818–1829.

Danard, M. B., 1964: On the influence of released latent heat on cyclone development. *J. Appl. Meteor.,* **3,** 27–37.

Doyle, J. D., and T. T. Warner, 1993: A numerical investigation of coastal frontogenesis and mesoscale cyclogenesis during GALE IOP 2. *Mon. Wea. Rev.,* **121,** 1048–1077.

Fantini, M., 1990: The influence of heat and moisture fluxes from the ocean on the developement of baroclinic waves. *J. Atmos. Sci.,* **47,** 840–855.

Hack, J. J., and W. H. Schubert, 1986: Nonlinear response of atmospheric vortices to heating by organized cumulus convection. *J. Atmos. Sci.,* **43,** 1559–1573.

Holton, J. R., 1992: *An Introduction to Dynamic Meteorology.* 3d ed. Academic Press, 511 pp.

Huo, Z., D.-L. Zhang, and J. R. Gyakum, 1996: The life cycle of the intense IOP-14 storm during CASP II. Part II: Sensitivity simulations. *Atmos.–Ocean,* **34,** 81–102.

Joly, A., and A. J. Thorpe, 1990: Frontal instability generated by tropospheric potential vorticity anomalies. *Quart. J. Roy. Meteor. Soc.,* **116,** 525–560.

——, and Coauthors, 1997: The Fronts and Atlantic Storm-Track Experiment (FASTEX): Scientific objectives and experimental design. *Bull. Amer. Meteor. Soc.,* **78,** 1917–1940.

Kain, J. S., and J. M. Fritsch, 1993: Convective parameterization for mesoscale models: The Kain–Fritsch scheme. *The Representation of Cumulus Convection in Numerical Models, Meteor. Monogr.,* No. 46, Amer. Meteor. Soc., 165–170.

Kuo, Y.-H., and S. Low-Nam, 1990: Prediction of nine explosive cyclones over the western Atlantic with a regional model. *Mon. Wea. Rev.,* **118,** 3–25.

——, M. A. Shapiro, and E. G. Donall, 1991: The interaction between baroclinic and diabatic processes in a numerical simulation of

a rapidly intensifying extratropical marine cyclone. *Mon. Wea. Rev.*, **119,** 368–384.
Lapenta, W. M., and N. L. Seaman, 1992: A numerical investigation of east coast cyclogenesis during the cold-air damming event of 27–28 February 1982. Part II: Importance of physical mechanisms. *Mon. Wea. Rev.*, **120,** 52–76.
Lupo, A. R., P. J. Smith, and P. Zwack, 1992: A diagnosis of the explosive development of two extratropical cyclones. *Mon. Wea. Rev.*, **120,** 1490–1523.
Mailhot, J., and C. Chouinard, 1989: Numerical forecasts of explosive winter storms: Sensitivity experiments with a meso-α scale model. *Mon. Wea. Rev.*, **117,** 1311–1342.
Mak, M., 1998: Influence of surface sensible heat flux on incipient marine cyclogenesis. *J. Atmos. Sci.*, **55,** 820–834.
Moore, G. W. K., and W. R. Peltier, 1987: Cyclogenesis in frontal zones. *J. Atmos. Sci.*, **44,** 384–409.
Mullen, S. L., 1982: Cyclone development in polar air streams over the wintertime continent. *Mon. Wea. Rev.*, **110,** 1664–1676.
——, and D. P. Baumhefner, 1989: The impact of initial condition uncertainty on numerical simulations of large-scale explosive cyclogenesis. *Mon. Wea. Rev.*, **117,** 2800–2821.
Nakamura, N., 1988: Scale selection of baroclinic instability—Effects of stratification and nongeostrophy. *J. Atmos. Sci.*, **45,** 3253–3267.
Newton, C. W., and E. O. Holopainen, Eds., 1990: *Extratropical Cyclones: The Erik Palmén Memorial Volume.* Amer. Meteor. Soc., 262 pp.
Orlanski, I., 1986: Localized baroclinicity: A source for meso-α cyclones. *J. Atmos. Sci.*, **43,** 2857–2885.
Petterssen, S., D. L. Bradbury, and K. Pedersen, 1962: The Norwegian cyclone models in relation to heat and cold sources. *Geofys. Publ.*, **24,** 243–280.
Reed, R. J., and A. J. Simmons, 1991: An explosively deepening cyclone over the North Atlantic that was unaffected by concurrent surface energy fluxes. *Wea. Forecasting,* **6,** 117–122.
——, Y.-H. Kuo, and S. Low-Nam, 1994: An adiabatic simulation of the ERICA IOP 4 storm: An example of quasi-ideal frontal cyclone development. *Mon. Wea. Rev.*, **122,** 2688–2708.
Schär, C., and H. Davies, 1990: An instability of mature cold fronts. *J. Atmos. Sci.*, **47,** 929–950.
Snyder, C., 1996: Summary of an informal workshop on adaptive observations and FASTEX. *Bull. Amer. Meteor. Soc.*, **77,** 953–961.
Thorncroft, C. D., and B. J. Hoskins, 1990: Frontal cyclogenesis. *J. Atmos. Sci.*, **47,** 2317–2336.
Tsou, C. H., and P. J. Smith, 1990: The role of synoptic/planetary scale interaction during the development of a blocking anticyclone. *Tellus*, **42A,** 763–786.
Zhang, D.-L., 1989: The effect of parameterized ice microphysics on the simulation of vortex circulation with a mesoscale hydrostatic model. *Tellus*, **41A,** 132–147.
——, E. Radeva, and J. Gyakum, 1999: A family of frontal cyclones over the western Atlantic ocean. Part I: A 60-h simulation. *Mon. Wea. Rev.*, **127,** 1725–1744.
Zwack, P., and B. Okossi, 1986: A new method for solving the quasigeostrophic omega equation by incorporating surface pressure tendency data. *Mon. Wea. Rev.*, **114,** 655–666.